Cellular/Molecular

CCK+ Interneurons Contribute to Thalamus-Evoked Feed-Forward Inhibition in the Prelimbic Prefrontal Cortex

Aichurok Kamalova,* Kasra Manoocheri,* Xingchen Liu,* Sanne M. Casello, Matthew Huang, Corey Baimel, Emily V. Jang, Paul G. Anastasiades, David P. Collins, and Adam G. Carter
Center for Neural Science, New York University, New York, New York 10003

Interneurons in the medial prefrontal cortex (PFC) regulate local neural activity to influence cognitive, motivated, and emotional behaviors. Parvalbumin-expressing (PV+) interneurons are the primary mediators of thalamus-evoked feed-forward inhibition across the mouse cortex, including the anterior cingulate cortex, where they are engaged by inputs from the mediodorsal (MD) thalamus. In contrast, in the adjacent prelimbic (PL) cortex, we find that PV+ interneurons are scarce in the principal thalamorecipient layer 3 (L3), suggesting distinct mechanisms of inhibition. To identify the interneurons that mediate MD-evoked inhibition in PL, we combine slice physiology, optogenetics, and intersectional genetic tools in mice of both sexes. We find interneurons expressing cholecystokinin (CCK+) are abundant in L3 of PL, with cells exhibiting fast-spiking (fs) or non–fast-spiking (nfs) properties. MD inputs make stronger connections onto fs-CCK+ interneurons, driving them to fire more readily than nearby L3 pyramidal cells and other interneurons. CCK+ interneurons in turn make inhibitory, perisomatic connections onto L3 pyramidal cells, where they exhibit cannabinoid 1 receptor (CB1R) mediated modulation. Moreover, MD-evoked feed-forward inhibition, but not direct excitation, is also sensitive to CB1R modulation. Our findings indicate that CCK+ interneurons contribute to MD-evoked inhibition in PL, revealing a mechanism by which cannabinoids can modulate MD-PFC communication.

Key words: **cannabinoids; CCK+ interneurons; inhibition; prefrontal cortex; thalamus**

Significance Statement

Here, we use anatomy, slice physiology, and optogenetics to examine how mediodorsal (MD) thalamus evokes feed-forward inhibition in Layer 3 of the prelimbic subregion of the mouse prefrontal cortex (PFC). We first show that PV+ interneurons are relatively sparse in Layer 3 of prelimbic PFC, whereas CCK+ interneurons are prevalent, and we describe the properties of these cells. We then show how MD thalamus preferentially drives a subpopulation of fast-spiking CCK+ interneurons to fire more readily than nearby pyramidal cells and other interneurons. Lastly, we show that CCK+ interneurons make inhibitory connections onto pyramidal cells and both CCK+ and thalamus-evoked inhibition are modulated by CB1 receptors. Our findings identify a novel and unexpected role for CCK+ interneurons in thalamus-evoked inhibition in the PFC.

Introduction

The medial prefrontal cortex (PFC) and mediodorsal (MD) thalamus are reciprocally connected brain regions that control cognition, motivation, and emotion (Euston et al., 2012; Parnaudeau et al., 2018; Halassa and Sherman, 2019). GABAergic interneurons in the mouse PFC are activated by excitatory inputs from the thalamus and mediate feed-forward inhibition (FFI) onto pyramidal cells (Delevich et al., 2015; Collins et al., 2018; Anastasiades et al., 2021). These interneurons thus play a critical role in controlling activity within corticothalamic loops and contribute to associated behaviors such as working memory (Bolkan et al., 2017; Schmitt et al., 2017; Mukherjee et al., 2021). Dysfunction of PFC interneurons is also linked to

Received May 23, 2023; revised April 12, 2024; accepted April 18, 2024.
Author contributions: A.K., K.M., X.L., P.G.A., D.P.C., and A.G.C. designed research; A.K., K.M., X.L., S.M.C., M.H., C.B., E.V.J., P.G.A., and D.P.C. performed research; A.K., K.M., X.L., S.M.C., P.G.A., and D.P.C. analyzed data; A.K., K.M., X.L., P.G.A., and A.G.C. wrote the paper.
We thank the members of the Carter Lab for their helpful discussions and comments on the manuscript. We thank Sumaita Mahmood and Jane Choe for their technical help with histology and viral injections. This work was supported by NIH T32 MH019524 (K.M.), NIH R01 MH085974 (A.G.C.), and NIH U19 NS123714 (A.G.C.).
*A.K., K.M., and X.L. contributed equally to this work.
The authors declare no competing financial interests.
P.G.A.'s present address: Department of Translational Health Sciences, University of Bristol, Whitson Street, Bristol BS1 3NY.
Correspondence should be addressed to Adam G. Carter at adam.carter@nyu.edu.
https://doi.org/10.1523/JNEUROSCI.0957-23.2024

neuropsychiatric disorders, including schizophrenia, stress disorders, and depression (Lewis et al., 2012; Dienel and Lewis, 2019). However, the composition of interneurons in the PFC may differ from other cortical areas (Whissell et al., 2015; Kim et al., 2017), particularly in the prelimbic (PL) and infralimbic (IL) cortices, and the cell types responsible for MD-evoked FFI in these regions remain unclear.

The PFC and other cortices contain a variety of GABAergic interneurons, which occupy specific layers, express distinct markers, and display different morphology, physiology, and local connectivity (McGarry and Carter, 2016; Tremblay et al., 2016; Anastasiades et al., 2018; Cummings and Clem, 2020; Liu et al., 2020; Anastasiades and Carter, 2021). Three major populations of interneurons include cells expressing parvalbumin (PV+), somatostatin (SOM+), and 5HT3a receptors, with the latter including interneurons that express vasoactive intestinal peptide (VIP+; Rudy et al., 2011). In most cases, PV+ cells mediate feedforward inhibition, SOM+ cells mediate feedback inhibition, and VIP+ cells mediate disinhibition (Gabernet et al., 2005; Cruikshank et al., 2007; Silberberg and Markram, 2007; Atallah et al., 2012; Gentet et al., 2012). However, the density of these cells is distinct in the PFC, with fewer PV+ interneurons and more SOM+ interneurons (Whissell et al., 2015; Kim et al., 2017), hinting at distinct connectivity and functional roles.

The mediodorsal (MD) thalamus sends robust glutamatergic projections to several subregions of the PFC, including the PL and anterior cingulate cortex (ACC; Krettek and Price, 1977; Kuramoto et al., 2017). Within both PL and ACC, MD axons are primarily concentrated in Layer 1b (L1b) and Layer 3 (L3; Delevich et al., 2015; Collins et al., 2018). MD inputs make strong, excitatory synapses onto L3 pyramidal cells, which they can drive to fire, and also engage inhibitory networks. In PL, MD inputs to L1b preferentially engage VIP+ interneurons that mediate disinhibition (Anastasiades et al., 2021). In ACC, MD inputs to L3 activate PV+ interneurons to mediate FFI (Delevich et al., 2015), as found in sensory systems. However, the number of PV+ interneurons in PL appears to be much less than in ACC (Whissell et al., 2015; Kim et al., 2017), suggesting another class of interneuron may mediate MD-evoked FFI onto pyramidal cells in PL.

Cholecystokinin-expressing (CCK+) interneurons are a subpopulation of inhibitory cells that also express 5-HT3a receptors (Rudy et al., 2011). CCK+ interneurons are unique among cortical interneurons in expressing cannabinoid type 1 receptors (CB1R) on their axon terminals, with inhibitory output strongly modulated by cannabinoids (Katona et al., 1999; Wilson et al., 2001; Wilson and Nicoll, 2001). However, because pyramidal cells can also express low levels of CCK, CCK+ interneurons have been difficult to study (Taniguchi et al., 2011). This technical challenge is overcome using intersectional labeling methods to target interneurons over pyramidal cells (Dimidschstein et al., 2016). In IL, ventral hippocampal inputs to L5 robustly engage CCK+ interneurons to mediate cannabinoid-sensitive FFI (Liu et al., 2020). In PL, recent work indicates that CCK+ interneurons are present in L3 and play an important role in working memory (Nguyen et al., 2020). One possibility is that these cells may compensate for the lack of PV+ interneurons and may confer unique properties, such as cannabinoid sensitivity, to MD-evoked FFI.

Here, we use slice electrophysiology and optogenetics to examine the contributions of PV+, SOM+, VIP+, and CCK+ interneurons in MD-evoked FFI at L3 pyramidal cells in PL. We first determine that PV+ interneurons are sparse in L3 of PL, whereas SOM+, VIP+, and CCK+ interneurons are abundant. We characterize two classes of CCK+ interneurons, which display either fast-spiking (fs) or non–fast-spiking (nfs) properties. We show that MD inputs drive robust action potential firing in fs-CCK+ interneurons more readily than pyramidal cells and other interneurons. We also establish that CCK+ interneurons robustly inhibit the soma of L3 pyramidal cells and that these connections are potently suppressed by CB1R modulation. Lastly, we show that MD-evoked FFI is also sensitive to CB1R modulation, indicating that CCK+ interneurons are likely major sources of FFI. These results highlight the physiology, connectivity, and functional properties of CCK+ interneurons in superficial layers of PL, which both contribute to MD-evoked FFI at L3 pyramidal cells and exhibit prominent sensitivity to cannabinoid signaling.

Materials and Methods

Animals

Experiments used wild-type and transgenic mice of either sex in a C57BL/6J background (all breeders from The Jackson Laboratory). Homozygote male breeders: PV-Cre = JAX 008069 (Hippenmeyer et al., 2005); SOM-Cre = JAX 013044 (Taniguchi et al., 2011); VIP-Cre = JAX 010908 (Taniguchi et al., 2011); CCK-Cre = JAX 012706 (Taniguchi et al., 2011); and PV-2A-Cre = JAX 012358 (Madisen et al., 2010) were paired with female wild-type or Ai14 (Cre-dependent tdTomato) breeders, JAX 007914 (Madisen et al., 2010), to yield heterozygote offspring used for experiments. All experimental procedures were approved by the University Animal Welfare Committee of New York University.

Viruses

Adeno-associated viruses (AAVs) used in this study were as follows: AAV1-hSyn-hChR2(H134R)-eYFP-WPRE-hGH (UPenn AV-26973P), AAV1-EF1a-DIO-eYFP-WPRE-hGH (UPenn AV-1-27056), AAV1-Dlx-Flex-EGFP (Addgene #83895; a gift from Jordane Dimidschstein and Gord Fishell; Dimidschstein et al., 2016), and AAV1-Dlx-Flex-ChR2-mCherry (a gift from Jordane Dimidschstein and Gord Fishell; Liu et al., 2020).

Stereotaxic injections

Mice aged 4–6 weeks were deeply anesthetized with isoflurane and then head-fixed in a stereotaxic frame (David Kopf Instruments). A small craniotomy was made over the injection site, using these coordinates relative to the bregma: PL PFC = ±0.4, −2.3, +2.1 mm; MD = −0.4, −3.5, −0.7 mm (mediolateral, dorsoventral, and rostrocaudal axes). Borosilicate pipettes with 5–10-µm-diameter tips were backfilled with virus, and a volume of 130–550 nl was pressure-injected using a Nanoject III (Drummond) every 30 s. The pipette was left in place for an additional 5 min, allowing time to diffuse away from the pipette tip, before being slowly retracted from the brain. For both retrograde and viral labeling, animals were housed for 2–3 weeks before slicing. We verified viral expression in the PFC and MD before use in slice electrophysiology recordings. Care was taken to avoid leakage into neighboring structures, but we cannot rule out some minor spread into PVT.

Histology and fluorescence microscopy

Mice were anesthetized with a lethal dose of ketamine and xylazine and then perfused intracardially with 0.01 M phosphate-buffered saline (PBS) followed by 4% paraformaldehyde (PFA) in 0.01 M PBS. Brains were fixed in 4% PFA in 0.01 M PBS overnight at 4°C. Slices were prepared at a thickness of 70 µm for directly imaging fluorescent proteins or tracers and 40 µm for antibody staining (Leica Vibratome Vt1000s). For immunohistochemistry, slices were incubated with blocking solution (1% bovine serum albumin and 0.2% Triton X-100 in 0.01 M PBS) for 1 h at room temperature before primary antibodies were applied in blocking solution [mouse anti-parvalbumin antibody (Millipore, MAB1572)] at 1:2,000 overnight at 4°C. Slices were then incubated with secondary antibodies in blocking solution [goat anti-mouse 647 at

1:200 (Invitrogen)] for 1.5 h at room temperature before mounting under glass coverslips on gelatin-coated slides using ProLong Gold antifade reagent with DAPI (Invitrogen). Images were acquired using a confocal microscope (Leica SP8). Image processing involved adjusting brightness, contrast, and manual cell counting using ImageJ (NIH).

Fluorescence in situ hybridization (RNAscope)

Mice were anesthetized with a lethal dose of ketamine and xylazine and then perfused intracardially with chilled 0.01 M PBS. Brains were immediately submerged in cold isopentane on dry ice after dissection. Solid brains were then embedded in OCT media (Tissue-Tek), frozen in isopentane, and stored in an airtight container at −80°C until sectioning. Sectioning was performed on a cryostat at −13°C, and 16 µm slices were mounted on Superfrost Plus microscope slides (Fisher Scientific) and stored at −80°C until staining. We followed a standardized RNAscope protocol for flash-frozen tissue from ACDBio, using Mm-Cck-C2, EGFP-C2, Mm-Pvalb-C3, Mm-VIP-C3, Mm-Cnr1-C3, and Mm-SST-C3 probes. Slides were mounted using ProLong Gold antifade reagent with DAPI (Invitrogen) before being covered under coverslips.

Slice preparation

Mice aged 6–8 weeks were anesthetized with an intraperitoneal injection of a lethal dose of ketamine and xylazine and perfused intracardially with an ice-cold external solution containing the following (in mM): 65 sucrose, 76 NaCl, 25 $NaHCO_3$, 1.4 NaH_2PO_4, 25 glucose, 2.5 KCl, 7 $MgCl_2$, 0.4 Na-ascorbate, and 2 Na-pyruvate (295–305 mOsm) and bubbled with 95% O_2/5% CO_2. Coronal slices (300 µm thick) were cut on a VS1200 vibratome (Leica) in ice-cold external solution and transferred to ACSF containing the following (in mM): 120 NaCl, 25 $NaHCO_3$, 1.4 NaH_2PO_4, 21 glucose, 2.5 KCl, 2 $CaCl_2$, 1 $MgCl_2$, 0.4 Na-ascorbate, and 2 Na-pyruvate (295–305 mOsm), bubbled with 95% O_2 / 5% CO_2. Slices were kept for 30 min at 35°C and recovered for 30 min at room temperature before starting recordings. All recordings were conducted at 30–32°C.

Electrophysiology

Whole-cell recordings were obtained from pyramidal cells or interneurons located in L3 of PL, defined as 225–300 µm from the pial surface (Collins et al., 2018). Cells were identified by infrared-differential interference contrast or fluorescence, as previously described (Chalifoux and Carter, 2010). Pairs of adjacent cells were chosen for sequential recording, ensuring they received similar inputs (typically <50 µm between cells). Borosilicate pipettes (3–5 MΩ) were filled with one of three internal solutions. For current-clamp recordings (in mM): 135 K-gluconate, 7 KCl, 10 HEPES, 10 Na-phosphocreatine, 4 Mg_2-ATP, 0.5 EGTA, and 0.4 Na-GTP, 290–295 mOsm, pH 7.3, with KOH. For voltage-clamp recordings (in mM): 135 Cs-gluconate, 10 HEPES, 0.5 EGTA, 10 Na-phosphocreatine, 4 Mg_2-ATP, and 0.4 Na-GTP, 10 TEA-chloride, and 2 QX-314, 290–295 mOsm, pH 7.3, with CsOH. For DSI and CB1R modulation experiments (in mM): 130 K-gluconate, 10 HEPES, 1.1 EGTA, 10 Na-phosphocreatine, 1.5 $MgCl_2$, 2 Mg_2-ATP, 0.4 Na-GTP. In some experiments studying cellular morphology, 5% biocytin was also included in the recording internal solution. After allowing biocytin to diffuse through the recorded cell for at least 30 min, slices were fixed with 4% PFA before staining with streptavidin conjugated to Alexa Fluor 647 (Invitrogen).

Electrophysiology recordings were made with a MultiClamp 700B amplifier (Axon Instruments), filtered at 4 kHz for current-clamp, and 2 kHz for voltage-clamp, and sampled at 10 kHz. The initial series resistance was <20 MΩ, and recordings were ended if the series resistance rose above 25 MΩ. In many experiments, 10 µM CPP was used to block NMDA receptors. In current-clamp experiments characterizing intrinsic properties, 10 µM NBQX, 10 µM CPP, and 10 µM gabazine were used to block excitation and inhibition. In some experiments, 10 µm AM-251 was used to block CB1 receptors, or 1 µM WIN 55,212–2 (WIN) was used to activate CB1 receptors. All chemicals were purchased from either Sigma or Tocris Bioscience.

Optogenetics

Channelrhodopsin-2 (ChR2) was expressed in presynaptic cells and activated with a 2 ms light pulse from a blue LED (473 nm; Thorlabs). For wide-field illumination, the light was delivered via a 10 × 0.3 NA objective (Olympus) centered on the recorded cell, as previously described (Collins et al., 2018; Liu et al., 2020; Anastasiades et al., 2021; Baimel et al., 2022; Manoocheri and Carter, 2022). LED power was routinely calibrated at the back aperture of the objective. LED power was adjusted to obtain reliable responses, with typical values of 0.4–10 mW. Subcellular targeting recordings utilized a digital mirror device (Mightex Polygon 400 G) to stimulate a 10 × 10 grid of 75 µm squares at a power range of 0.05–0.2 mW per square at 1 Hz, with the first row aligned to the pia, as previously described (Manoocheri and Carter, 2022).

Data analysis

Electrophysiology and imaging data were acquired using National Instruments boards and custom software written in MATLAB (MathWorks). Offline analysis was performed using custom software written in Igor Pro (WaveMetrics). Intrinsic properties were determined as follows. Input resistance was calculated from the steady-state voltage during a −50 pA, 500 ms current step. The maximum firing rate was determined by increasing the current injection in a stepwise fashion until the firing rate plateaued. Rheobase was determined by the average minimum current injection that elicited firing. For experiments with a single optogenetic stimulation, the PSC amplitude was measured as the average value across 1 ms around the peak subtracted by the average 100 ms baseline value prior to the stimulation. For experiments with a train of optogenetic stimulation, each PSC amplitude was measured as the average value in a 1 ms window around the peak, minus the average 2 ms baseline value before each stimulation. Most summary data are reported in the text and figures as arithmetic mean ± SEM. Ratios of responses at pairs of cells are reported as geometric mean in the text and with ± 95% confidence interval (CI) in the figures, unless otherwise noted. Comparisons between unpaired data were performed using the nonparametric Mann–Whitney *U* test. Comparisons between data recorded in pairs were performed using the nonparametric Wilcoxon test. For unpaired comparisons of more than two groups, Kruskal–Wallis tests with Dunn's multiple-comparisons tests were performed. Two-tailed p values < 0.05 were considered significant.

Results

Parvalbumin-expressing interneurons are sparse in L3 of the prelimbic cortex

MD thalamus generates direct excitation and feed-forward inhibition (FFI) in both the PL and ACC subregions of the medial PFC (Delevich et al., 2015; Collins et al., 2018). To examine MD-evoked synaptic responses in PL, we injected AAV-ChR2-eYFP into MD, waited for expression and transport (Fig. 1*A*, Extended Data Fig. 1-1*A,B*). We then recorded light-evoked EPSCs at −60 mV, the reversal potential for inhibition, and IPSCs at +10 mV, the reversal potential for excitation, from L3 pyramidal cells (Fig. 1*B*). Consistent with our previous work (Collins et al., 2018), we found that MD inputs evoke prominent excitation and FFI (EPSC = 335 ± 22 pA, IPSC = 391 ± 101 pA; $n = 8$ cells, three animals; Fig. 1*B,C*). MD-evoked FFI exhibited a delay (EPSC to IPSC = 2.8 ± 0.8 ms, $n = 8$ cells, three animals) and displayed a pronounced reduction of amplitude [paired-pulse ratio (PPR) = $IPSC_5/IPSC_1 = 0.04 \pm 0.01$, $n = 8$ cells, three animals; Fig. 1*B,C*], as observed for FFI mediated by PV+ interneurons in other cortical regions (Gabernet et al., 2005; Cruikshank et al., 2010).

PV+ interneurons have been shown to mediate MD-evoked FFI in ACC (Delevich et al., 2015), but whether this occurs in PL is unknown. While PV+ interneurons are the most abundant GABAergic cell type in most of the cortex (Rudy et al., 2011), recent work suggests a relative paucity of PV+ interneurons in

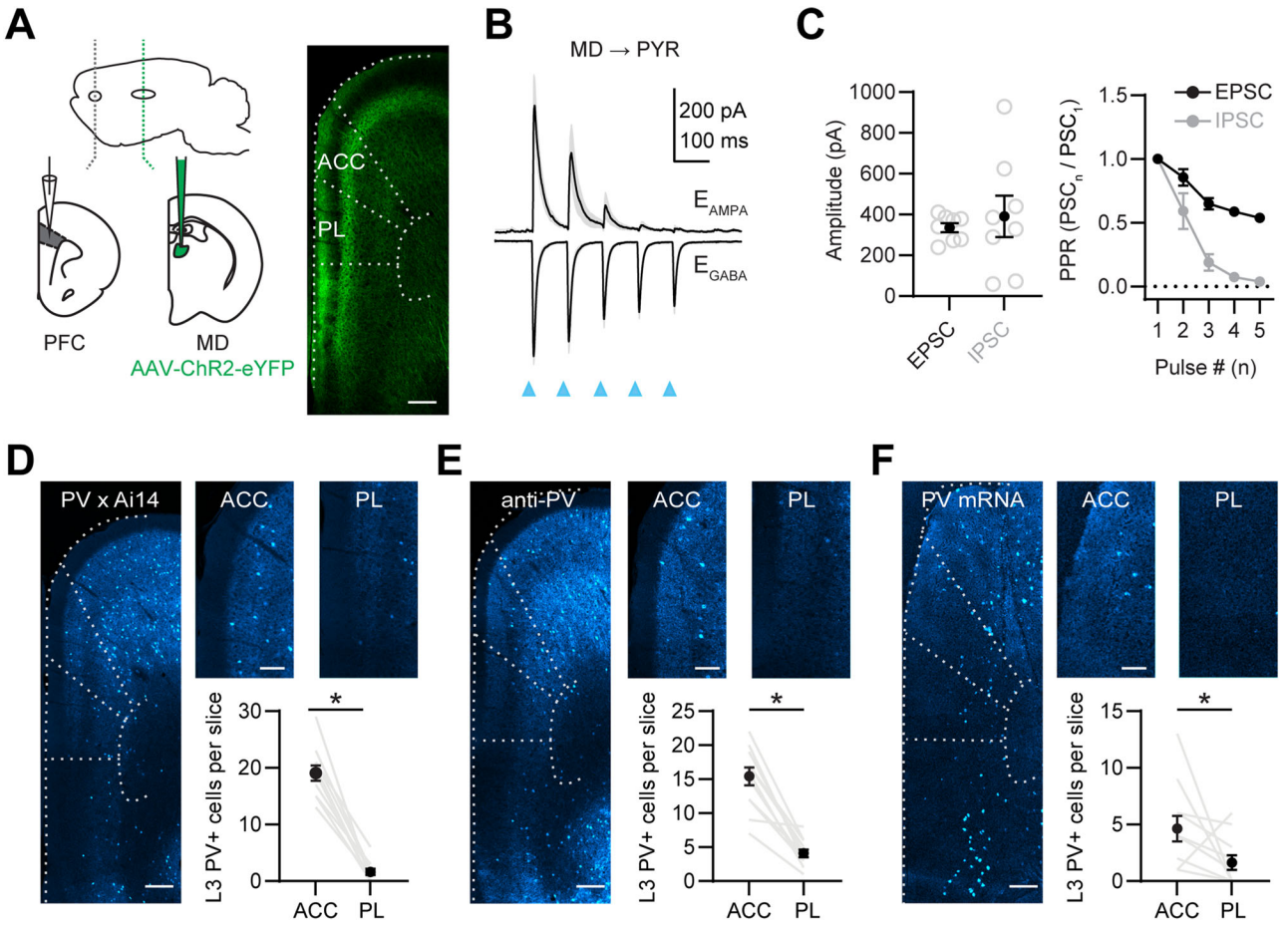

Figure 1. PV+ interneurons are sparse in L3 of PL. ***A***, Left, Schematic of AAV-ChR2-eYFP injection into MD and recording from the ipsilateral PFC. Right, Labeling of MD axons in L1b and L3 of the PFC, including the prelimbic (PL) and anterior cingulate cortex (ACC). Dashed lines = subregion borders. Scale bar = 200 µm. ***B***, Average MD-evoked EPSCs (at $E_{GABA} = -60$ mV) and IPSCs (at $E_{AMPA} = +10$ mV) at L3 pyramidal cells (PYR; $n = 8$ cells, three animals). Blue arrow = 2 ms light pulse. ***C***, Left, Summary of MD-evoked EPSC and IPSC amplitudes, where gray dots are individual cells. Right, Summary of paired-pulse ratio (PPR = PSC_n/PSC_1) for MD-evoked responses as a function of pulse number (n). ***D***, Left, Confocal image of labeled cells (blue) in PV-Cre x Ai14 mice, across the dorsoventral axis of the PFC. Dashed lines = subregion borders. Scale bar = 200 µm. Right top, Expansion of ACC (left) and PL (right), showing differential labeling. Scale bar = 100 µm. Right bottom, Summary of labeling in L3 of ACC and PL, with minimal labeling in the latter. Gray lines = individual slices ($n = 11$ slices, three animals). ***E***, Similar to ***D*** for anti-PV antibody labeling ($n = 12$ slices, three animals). ***F***, Similar to ***E*** for PV RNA labeling ($n = 11$ slices, three animals).

PL compared with other cortical areas (Kim et al., 2017). Whether this relative lack of PV+ interneurons in PL occurs within the main thalamorecipient L3 was unclear. Therefore, we next used three separate methods to visualize PV+ interneurons and compared their distributions across cortical layers in both PL and ACC. First, we labeled PV+ interneurons using PV-Cre mice crossed with Ai14 reporter mice to express Cre-dependent tdTomato in PV+ cells (Madisen et al., 2010). We found significantly fewer PV+ interneurons labeled in PL L3 relative to ACC L3 (PL L3 PV x Ai14 = 1.6 ± 0.5 cells per slice, ACC L3 PV x Ai14 = 19 ± 1.4, $p = 0.001$; $n = 11$ slices, three animals; Fig. 1*D*, Extended Data Fig. 1-1*C,D*). To confirm the lack of PV+ interneurons is not due to reduced expression of Cre in these mice, we also compared PV labeling with immunohistochemistry and fluorescence in situ hybridization (RNAscope; Wang et al., 2012; Fig. 1*E,F*). We found that both immunolabeled (PL L3 PV = 4.1 ± 0.6 cells per slice, ACC L3 PV = 15.4 ± 1.3, $p = 0.0005$; $n = 12$ slices, three animals) and mRNA labeled (PL L3 PV = 1.6 ± 0.7 cells per slice, ACC L3 PV = 4.6 ± 1.1, $p = 0.035$; $n = 11$ slices, three animals) PV+ interneurons were significantly less abundant in PL L3 compared with ACC L3. However, there was significantly higher PV labeling in PL L5 compared with L3 (Extended Data Fig. 1-1*E–G*). These results show a relative lack of PV+ interneurons in PL L3, suggesting another interneuron is responsible for MD-evoked FFI.

CCK-expressing interneurons are prominent in L3 of the prelimbic cortex

While PV+ interneurons are common across the cortex, several other cell types are also abundant and could contribute to MD-evoked FFI. We next used transgenic mice and viruses to establish the distributions of SOM+, VIP+, and CCK+ interneurons in L3 of PL (Fig. 2*A*). We labeled SOM+ and VIP+ interneurons by crossing Cre lines with a Cre-dependent tdTomato reporter line (Ai14; Madisen et al., 2010). We labeled CCK+ interneurons by injecting a Cre-dependent, interneuron-specific virus expressing EGFP (AAV-Dlx-Flex-EGFP) into the PFC of CCK-Cre mice, which minimizes expression in pyramidal cells that can express low levels of CCK (Dimidschstein et al., 2016). We observed higher numbers of SOM+, VIP+, and CCK+ interneurons compared with PV+ interneurons in L3 of PL (PV+ = 2.3 ± 0.5 cells per slice, SOM+ = 13.5 ± 0.9, VIP+ = 14.3 ± 0.7, CCK+ = 9.5 ± 1; PV vs SOM, $p < 0.0001$, PV vs VIP, $p < 0.0001$; PV vs CCK, $p = 0.032$; $n = 12$ slices, three animals each; Fig. 2*B,C*).

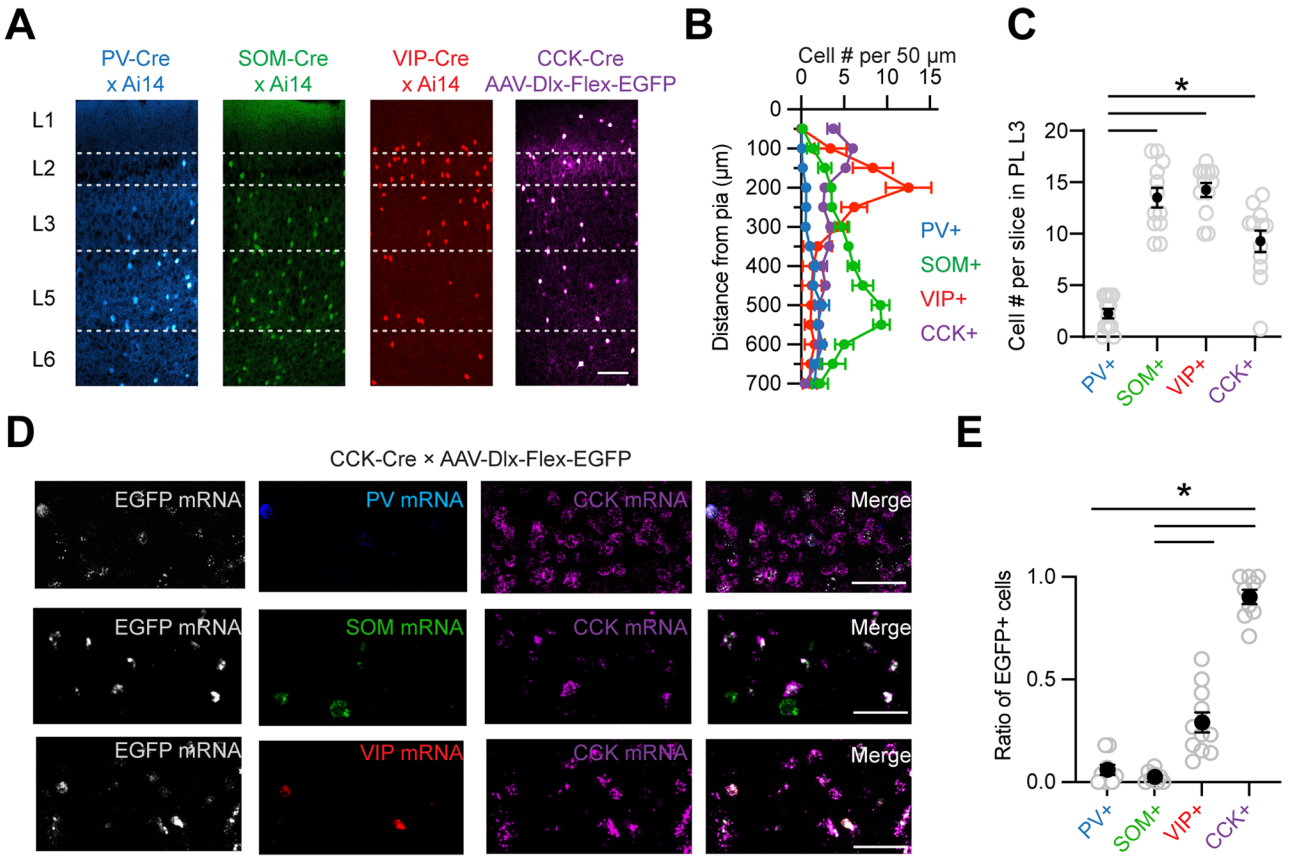

Figure 2. CCK+ interneurons are prominent in L3 of PL. ***A***, Confocal images of GABAergic interneurons across layers of PL. From left to right, PV+ interneurons labeled in PV-Cre x Ai14 mice; SOM+ interneurons labeled in SOM-Cre x Ai14 mice; VIP+ interneurons labeled in VIP-Cre x Ai14 mice, and CCK+ interneurons labeled by injecting AAV-Dlx-Flex-EGFP virus into CCK-Cre mice. Dashed lines = layer borders. Scale bar = 100 µm. ***B***, Average number of each interneuron across cortical depth ($n = 12$ slices, three animals each). ***C***, Summary of the average number of labeled cells in each PL L3 slice. Open circles = individual slices. ***D***, Confocal images of RNA staining in L3 PL of CCK-Cre mice injected with AAV-Dlx-Flex-EGFP virus. Each slice was stained for EGFP, PV, SOM, VIP, and/or CCK mRNA. Scale bar = 100 µm. ***E***, Summary of overlap between EGFP+ (white) and PV+ (blue), SOM+ (green), VIP+ (red), or CCK+ (magenta) mRNA (EGFP+/CCK+: $n = 9$ slices, three animals; EGFP+/PV+: $n = 9$ slices, three animals; EGFP+/SOM+: $n = 8$ slices, three animals; EGFP+/VIP+: $n = 11$ slices, five animals). Open circles = individual slices. Values are mean ± SEM. *$p < 0.05$.

These results suggest all three classes of GABAergic interneurons are well positioned to mediate MD-evoked FFI in L3 of PL.

We were particularly interested in the CCK+ interneurons, which we recently showed contribute to hippocampal-evoked FFI in Layer 5 of the IL PFC (Liu et al., 2020). To validate our ability to specifically label CCK+ interneurons, we examined mRNA expression of known interneuron markers using fluorescence in situ hybridization (RNAscope; Fig. 2*D*,*E*). In CCK-Cre mice injected with AAV-Dlx-Flex-EGFP, we found that EGFP+ cells exhibited significant overlap with CCK+ mRNA (EGFP+/CCK+ = 0.90 ± 0.03, $n = 9$ slices, three animals) but minimal overlap with either PV+ mRNA (EGFP+/PV+ = 0.08 ± 0.03, $n = 9$ slices, three animals) or SOM+ mRNA (EGFP+/SOM+ = 0.03 ± 0.03, $n = 8$ slices, three animals). We also found a small population of EGFP+ cells that overlapped with VIP+ mRNA (EGFP+/VIP+ = 0.29 ± 0.05, $n = 11$ slices, five animals), consistent with previous reports (Bodor et al., 2005; Tasic et al., 2018; Gouwens et al., 2020; (BICCN), 2021; Scala et al., 2021), and suggesting heterogeneity in the CCK+ population. These results indicate our approach reliably labels CCK+ interneurons, with minimal labeling of other cell types, enabling us to assess how they are engaged by MD inputs and contribute to FFI in PL.

PL L3 interneurons have characteristic intrinsic properties

Having identified several interneurons as possible candidates for mediating inhibition in PL L3, we next sought to characterize their intrinsic properties. While we previously assessed the intrinsic properties of CCK+ interneurons in deep layers of the neighboring IL PFC (Liu et al., 2020), the intrinsic properties of PL L3 CCK+ interneurons have remained unknown. We used whole-cell current-clamp recordings in coronal slices to characterize the morphology and physiology of PV+, SOM+, VIP+, and CCK+ interneurons in PL L3 (Fig. 3*A*,*B*). We found that PV+, SOM+, and VIP+ interneurons had similar intrinsic properties to those previously reported in the PFC and other cortices (McGarry et al., 2010; Lee et al., 2013; Karnani et al., 2016), consistent with studies of the diversity of inhibitory cell types throughout the cortex (Tasic et al., 2018; Gouwens et al., 2020; (BICCN), 2021; Scala et al., 2021). Interestingly, CCK+ interneurons in L3 of PL showed two strikingly divergent subtypes (Fig. 3*B*,*C*): (1) fast-spiking CCK+ (fs-CCK+) interneurons with a high max firing rate, high rheobase, and low input resistance (max firing rate = 248 ± 18 Hz; rheobase = 351 ± 67 pA; input resistance = 103 ± 13 MΩ, $n = 7$ cells, four animals) and (2) non–fast-spiking CCK+ (nfs-CCK+) interneurons with low max firing rate, low rheobase, and high input resistance (max firing rate = 64 ± 11 Hz; rheobase = 98 ± 29 pA; input resistance = 377 ± 84 MΩ, $n = 7$ cells, four animals). We distinguished fs-CCK+ from nfs-CCK+ interneurons by determining their maximal firing rate and applying a cutoff of 100 Hz. These results are consistent with previous studies of CCK+ interneurons in other cortical areas, which identified both fast-spiking basket

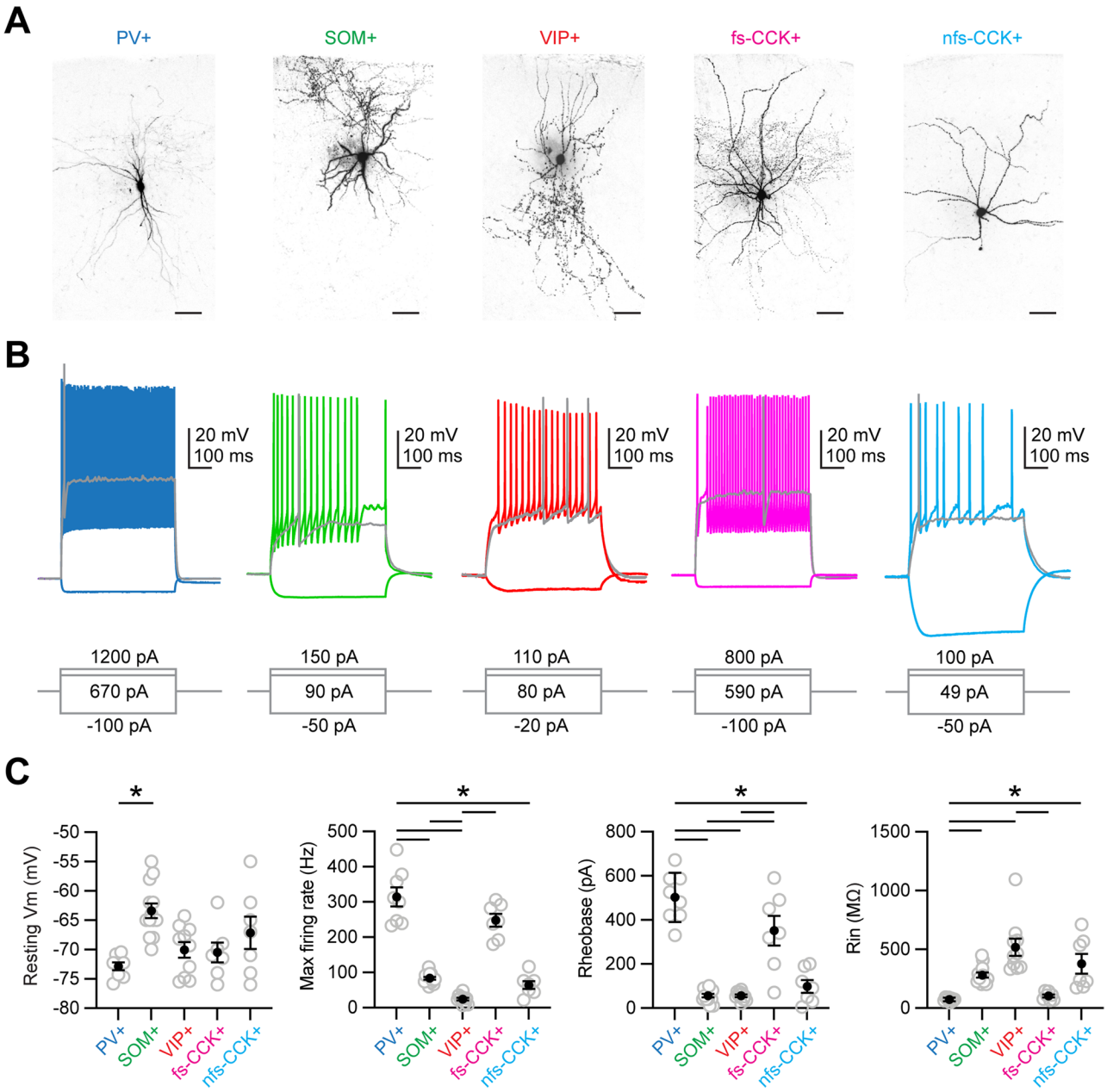

Figure 3. Distinct intrinsic properties of L3 interneurons. ***A***, Representative biocytin fills showing the morphology of recorded PV+, SOM+, VIP+, fast-spiking CCK+ (fs-CCK+), and non–fast-spiking CCK+ (nfs-CCK+) interneurons. Scale bar = 50 µm. ***B***, AP firing in response to current injection at rheobase (gray traces) and max firing rate (colored traces), in addition to a hyperpolarizing current step for each cell type shown in ***A*** (note current steps not drawn to scale). ***C***, Summary of key intrinsic properties, including resting membrane potential (Vm), max firing rate, rheobase current, and input resistance (Rin; PV+: $n = 8$ cells, four animals; SOM+: $n = 13$ cells, three animals; VIP+: $n = 10$ cells, four animals; fs-CCK+: $n = 7$ cells, four animals; nfs-CCK+: $n = 7$ cells, four animals). Values are mean ± SEM. *$p < 0.05$.

cells and a population of highly excitable bipolar cells (Kawaguchi and Kubota, 1998; He et al., 2016). Notably, the intrinsic properties of fs-CCK+ interneurons are broadly similar to PV+ interneurons that mediate thalamus-evoked inhibition in other parts of the cortex (Porter et al., 2001).

Thalamic inputs preferentially drive fs-CCK+ interneurons in PL L3

While PV+ interneurons in other cortical areas receive strong thalamic input and often act as the primary mediator of FFI (Cruikshank et al., 2007), their low numbers in PL L3 suggest other interneuron cell types could be fulfilling that role in this circuit. We next examined which population of interneurons are preferentially activated by MD inputs, assessing which cell types are activated more readily than neighboring L3 pyramidal cells, which is the hallmark of FFI. To study MD-evoked activity, we injected AAV-ChR2-eYFP into MD while also labeling PV+, SOM+, VIP+, or CCK+ interneurons. After waiting for expression and transport, we prepared coronal PFC slices and made sequential recordings from neighboring pairs of L3 pyramidal cells and either PV+, SOM+, VIP+, or CCK+ interneurons at their resting membrane potential (Fig. 4*A*). We activated MD inputs with a stimulus train (five pulses at 10 Hz, 2 ms pulse duration) at several light intensities (1–8 mW; Fig. 4*B*, Extended Data Fig. 4-1). To compensate for variation in viral labeling, we compared firing probability at the lowest intensity

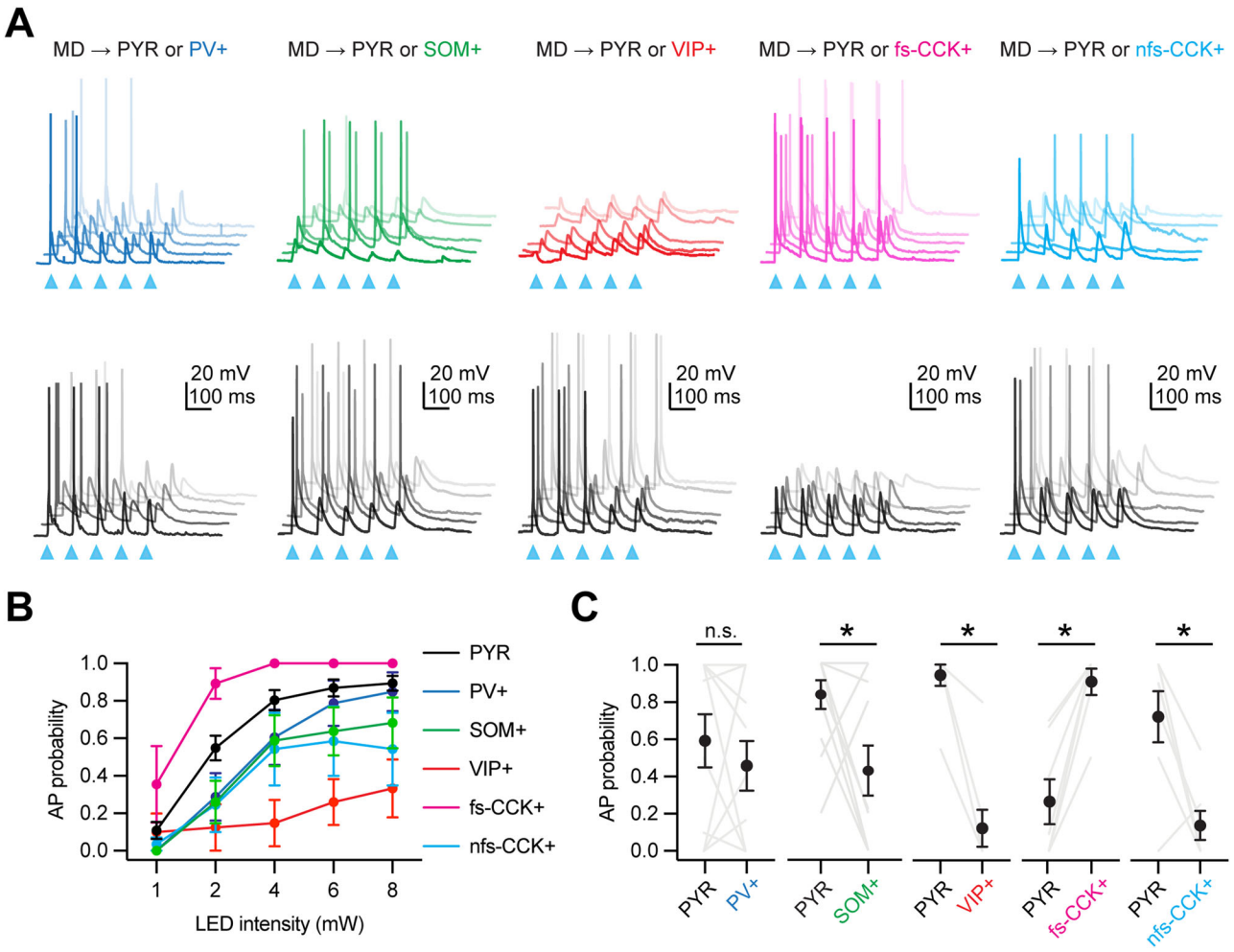

Figure 4. MD preferentially activates fast-spiking CCK ± interneurons. ***A***, MD-evoked EPSPs and APs at pairs of interneurons (color, top) and corresponding PYR (black, bottom), showing PV+, SOM+, VIP+, fs-CCK+, and nfs-CCK+ interneurons, with five example traces offset for each cell. Replicates are denoted by different colors. Blue arrow = 2 ms light pulse. ***B***, Summary of AP probability at any stimulus pulse during trains across five different light intensities, color-coded as in ***A*** (PV+: $n = 11$ pairs, five animals; SOM+: $n = 12$ pairs, four animals; VIP+: $n = 8$ pairs, four animals; fs-CCK+: $n = 7$ pairs, five animals; nfs-CCK+: $n = 7$ pairs, four animals). ***C***, Summary of AP probability during trains at the lowest light intensity that drove firing at either the interneuron or PYR in a pair, color-coded as in (***A***). Values are mean ± SEM. $*p < 0.05$ (Extended Data Fig. 4-1).

that reliably drove firing in at least one cell type in the pair (Fig. 4*C*). Because each pair used a different light intensity, the firing probability was variable across recordings, leading to different firing of pyramidal cells. However, we found that only fs-CCK+ interneurons were activated at lower intensities relative to L3 pyramidal cells, whereas PV+ interneurons were activated at similar intensities to L3 pyramidal cells, and SOM+, VIP+, and nfs-CCK+ interneurons were only engaged when L3 pyramidal cells were already active (Fig. 4*C*; firing probabilities: L3 PYR vs L3 PV+ = 0.59 ± 0.14 vs 0.46 ± 0.13, $p = 0.43$, $n = 11$ pairs, five animals; L3 PYR vs L3 SOM+ = 0.83 ± 0.08 vs 0.43 ± 0.13, $p = 0.02$, $n = 12$ pairs, four animals; L3 PYR vs L3 VIP+ = 0.94 ± 0.06 vs 0.12 ± 0.10, $p = 0.008$, $n = 8$ pairs, four animals; L3 PYR vs L3 fs-CCK+ = 0.27 ± 0.12 vs 0.91 ± 0.07, $p = 0.03$, $n = 7$ pairs, five animals; L3 PYR vs L3 nfs-CCK+ = 0.72 ± 0.14 vs 0.14 ± 0.08, $p = 0.008$, $n = 7$ pairs, four animals). Examining responses over stimulus trains, we observed that MD-evoked firing was also highly adapting at fs-CCK+ interneurons (Extended Data Fig. 4-1), resembling the MD-evoked FFI observed at L3 pyramidal cells (Fig. 1*B*,*C*). Together, these results indicate MD input influences multiple interneuron populations in L3 of the PL PFC but preferentially drives fs-CCK+ interneurons to fire before L3 pyramidal cells, which could be replacing PV+ interneurons as the primary contributor to thalamus-evoked FFI.

We previously found that poor PV+ interneuron labeling in other brain regions can be overcome using the PV-2A-Cre transgenic line (Madisen et al., 2010; Scudder et al., 2018; Baimel et al., 2022). To test if this approach might also allow us to target a previously undetectable population of fast-spiking cells in the PFC, we injected AAV-Dlx-Flex-EGFP into the PL of PV-2A-Cre mice (Fig. 5). With this strategy, we observed a substantially greater number of labeled cells across layers of PL (Fig. 5*A*). However, in situ hybridization showed low colabelling of EGFP+ cells with PV+ mRNA and substantial labeling with CCK+ mRNA (Fig. 5*B*). Interestingly, current-clamp recordings showed these cells displayed a fast-spiking phenotype (max firing rate = 212 ± 13.6 Hz; rheobase = 300 ± 28.2 pA; input resistance = 105.7 ± 7.5 MΩ, $n = 10$ cells, four animals; Fig. 5*C*,*D*). Moreover, optogenetic experiments showed these cells could be driven to fire, similar to our PV-Cre recordings (Fig. 5*E*). However, unlike fs-CCK+ interneurons, there were no significant differences in firing probability compared with nearby L3 pyramidal neurons in response to MD inputs (Fig. 5*F*; firing probability: L3 PYR vs L3 PV-2A+ = 0.57 ± 0.14 vs 0.51 ± 0.16, $p = 0.81$, $n = 7$ pairs, three animals).

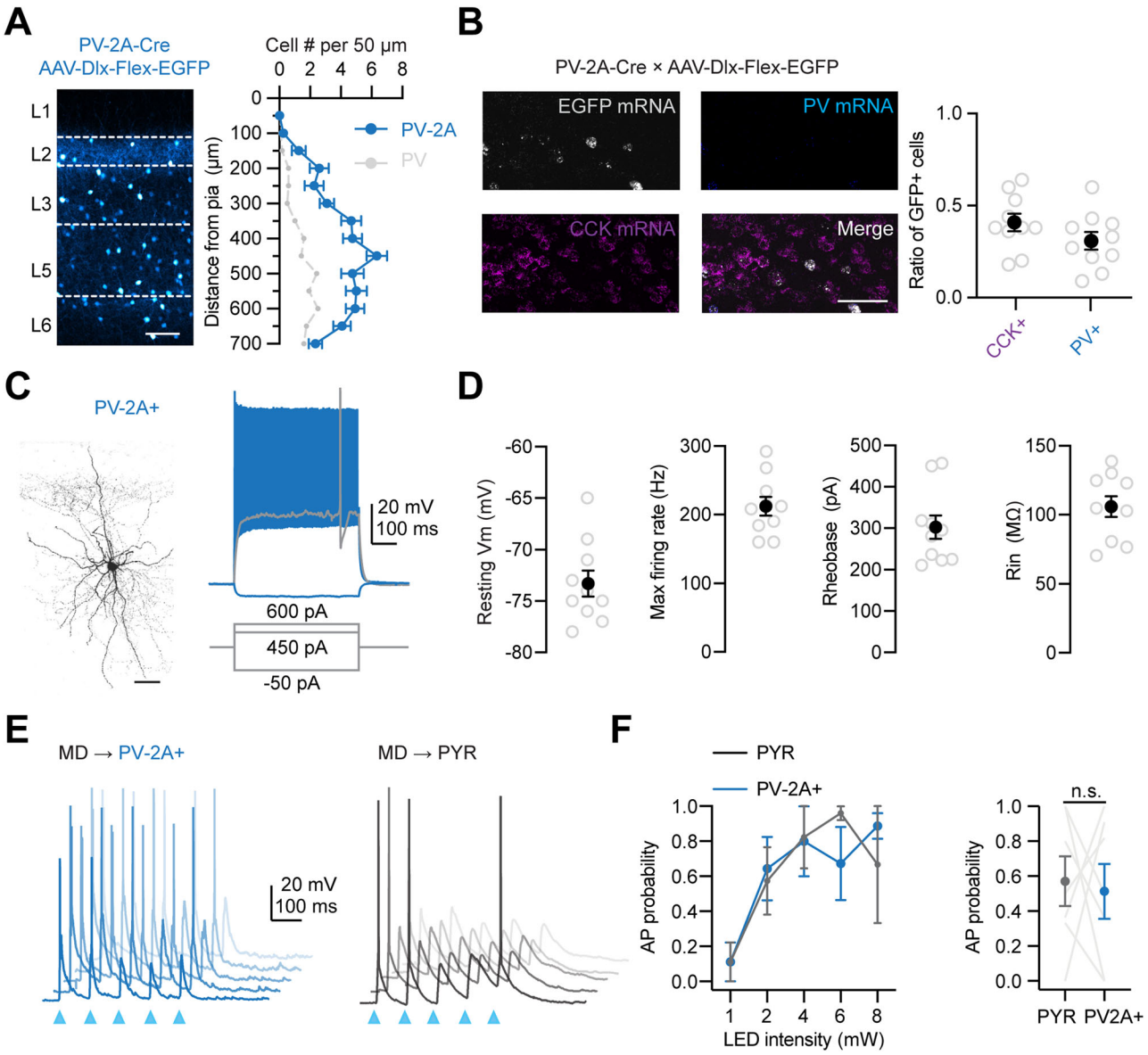

Figure 5. PV-2A-Cre labels both PV ± and CCK+ interneurons. ***A***, Left, Confocal images of labeled cells in PV-2A-Cre animal injected with AAV-Dlx-Flex-EGFP across PL layers. Dashed lines = layer borders. Scale bar = 100 µm. Right, Average number of PV-2A+ (blue) interneurons across cortical depth relative to PV+ interneuron distribution from PV x Ai14 (gray, same dataset as Fig. 2*A–C*). ***B***, Left, Confocal images of EGFP+, PV+, and CCK+ mRNA labeling in L3 of PL. Scale bar = 100 µm. Right, Summary of the overlap between EGFP+ and either CCK+ or PV+ mRNA (n = 9 slices, three animals). ***C***, Left, Representative biocytin fill showing morphology of L3 PV-2A+ interneuron. Scale bar = 100 µm. Right, Example firing pattern in response to current injection at rheobase (gray trace) and max firing rate (blue trace) in addition to a hyperpolarizing current step for PV-2A+ interneurons (note current steps are not drawn to scale). ***D***, Summary of key intrinsic properties, including resting membrane potential (Vm), max firing rate, rheobase current, and input resistance (Rin; n = 10 cells, four animals). ***E***, Examples of MD-evoked EPSPs and AP firing at pairs of PV-2A+ interneurons (blue) and PYR (gray) in L3, with five example traces shown for each cell. Blue arrow = 2 ms light pulse. ***F***, Left, Summary of AP probability at any stimulus pulse during trains across five different light intensities. Right, Summary of AP probability per pair of PV-2A+ interneuron and PYR in L3 during the stimulus train (n = 7 pairs, three animals).

Together, these results suggest PV-2A-Cre labels a complex selection of interneurons, which are unlikely to be the main mediator of MD-evoked FFI in PL.

CCK+ interneurons robustly inhibit L3 pyramidal cells in PL

Having identified CCK+ interneurons as a key target of MD, we next characterized their output onto L3 pyramidal cells in PL. Previous studies in the hippocampus and cortex indicate that CCK+ basket cells, analogous to fs-CCK+ interneurons, share some properties with PV+ basket cells, and thus could be performing a similar role in the PFC (Kawaguchi and Kubota, 1998; Armstrong and Soltesz, 2012). To test this idea, we first examined whether CCK+ output to PL L3 is GABAergic, using a Cre-dependent, interneuron-specific virus expressing ChR2 (AAV-Dlx-Flex-ChR2) injected into the PFC of CCK-Cre mice (Fig. 6*A*). In slice recordings, we stimulated CCK+ interneurons with brief light pulses (2 ms) and recorded L3 pyramidal cells held at −50 mV with a low chloride [Cl−] internal solution, which increases the driving force for $GABA_A$ receptor currents and simultaneously captures both EPSCs and IPSCs (Fig. 6*B*; Glickfeld and Scanziani, 2006). We found robust CCK-evoked IPSCs but not EPSCs, which were blocked by wash-in of the $GABA_A$ receptor antagonist, gabazine (10 µM; baseline IPSC = 218 ± 60 pA, gabazine IPSC = 1.5 ± 0.3 pA, p = 0.0078, n = 8 pairs, three animals; Fig. 6*B*). These results confirm that CCK+ interneuron output is

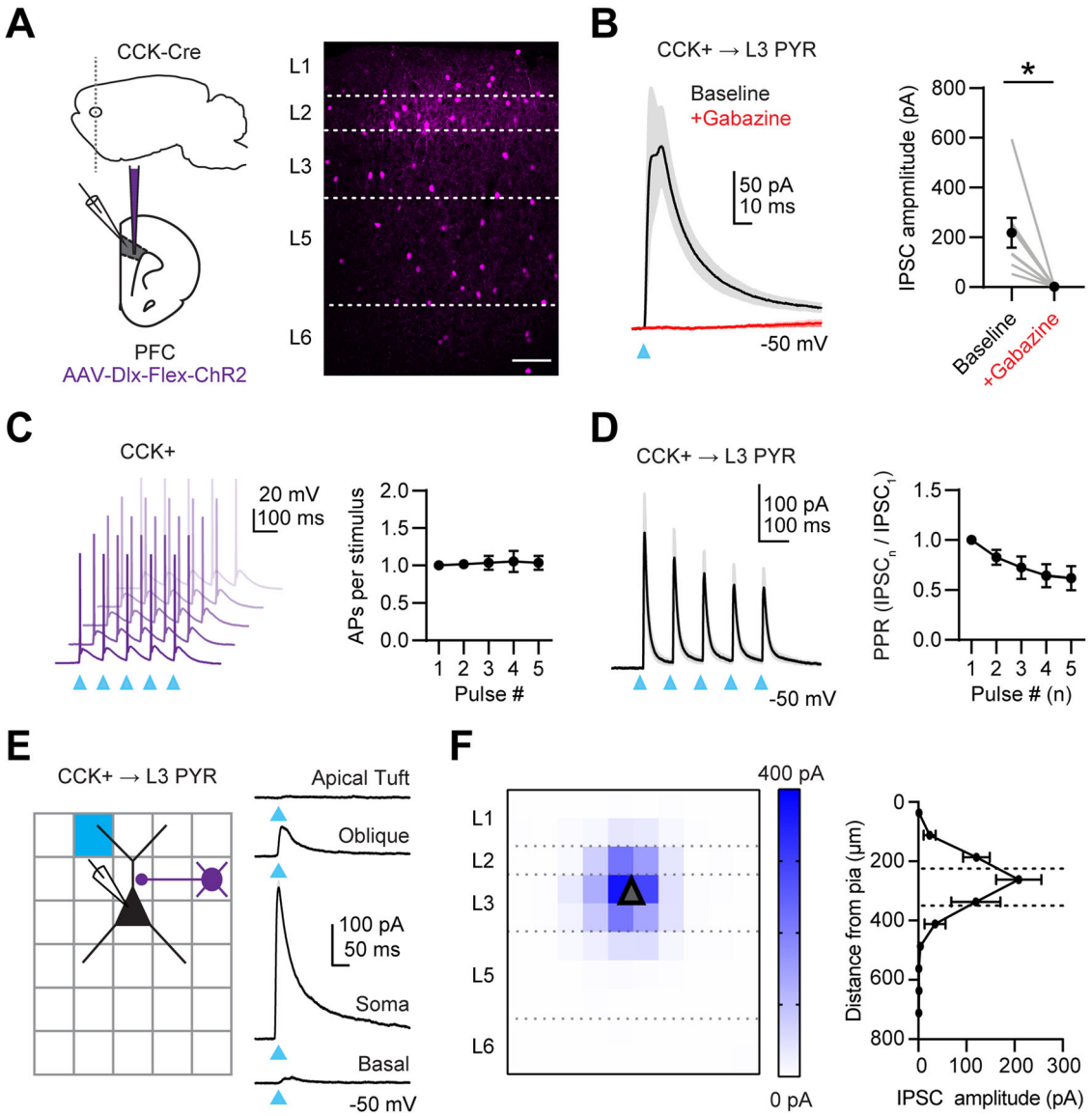

Figure 6. Properties of CCK ± synapses onto L3 pyramidal cells. ***A***, Left, Schematic of injection of AAV-Dlx-Flex-ChR2 into PL of CCK-Cre mice to express opsin in CCK+ interneurons. Right, Confocal image of CCK+ interneurons across layers. Dashed lines = layer borders. Scale bar = 100 µm. ***B***, Left, Average CCK-evoked IPSCs in PL L3 PYR at baseline (black) and after gabazine (red), recorded with low [Cl−] internal at −50 mV. Blue arrow = 2 ms light pulse. Right, Summary of IPSC amplitude before and after gabazine wash-in. The gray lines are individual cells ($n = 8$ cells, three animals). ***C***, Left, Example traces of CCK+ interneuron firing in response to 10 Hz light pulses. Blue arrow = 2 ms light pulse. Right, Summary of the number of APs per pulse of stimulation ($n = 7$ cells, four animals). ***D***, Left, Average CCK+-evoked IPSCs recorded at L3 PYRs at −50 mV with 10 Hz stimulation. Blue arrow = 2 ms light pulse. Right, Summary of paired-pulse ratio (PPR = IPSC$_n$/IPSC$_1$) across the stimulus train ($n = 7$ cells, four animals). ***E***, Left, Schematic for sCRACM experiment, with PL L3 PYR recorded at −50 mV in the presence of TTX and 4-AP and CCK + interneuron terminals stimulated in a 10 × 10 grid of 75 µm squares via patterned light. Right, Example CCK+-evoked IPSCs along the somatodendritic axis. Blue arrow = 2 ms light pulse. ***F***, Left, Summary of average IPSC amplitudes evoked across the 10 × 10 grid ($n = 8$ cells, three animals). Right, Summary of IPSC amplitudes as a function of distance to the pial surface ($n = 8$ cells, three animals). The dotted lines indicate L3. Values are mean ± SEM. * = $p < 0.05$.

exclusively inhibitory in PL L3 and that our approach targets inhibitory interneurons.

Another important property that affects CCK output to PL L3 is short-term synaptic dynamics, including whether they facilitate or depress (Zucker and Regehr, 2002). To examine the dynamics of CCK+ output to L3 pyramidal cells in PL, we next recorded pairs of CCK+ interneurons expressing ChR2 and a nearby L3 pyramidal cells, calibrating our stimulus intensity so that the CCK+ interneuron fired a single action potential per pulse (Fig. 6*C*). We found CCK+ synapses on PL L3 pyramidal cells exhibited marked depression (PPR = EPSC$_5$/EPSC$_1$ = 0.62 ± 0.05, n = 7 cells, four animals; Fig. 6*D*), similar to PV+ interneuron output in many other circuits (Reyes et al., 1998; Gabernet et al., 2005) and mirroring the depressing FFI we observed in the MD to PFC circuit. Lastly, the subcellular targeting of CCK+ synapses on pyramidal cells could affect their influence on activity in PL L3 (Marlin and Carter, 2014). Using subcellular channelrhodopsin-assisted circuit mapping (sCRACM; Petreanu et al., 2009), we recorded L3 pyramidal cells while stimulating across the layers of PL using a pseudorandom grid, under conditions that restrict synaptic transmission to direct terminal release (Fig. 6*E*). We found that CCK-evoked IPSCs were primarily targeted to the peri-somatic region ($n = 8$ cells, three animals; Fig. 6*E,F*), consistent with a substantial CCK+ basket cell population in PL L3, which may act analogously to L3 PV+ interneurons in ACC and other areas of the cortex. Together, these results show that CCK+ interneurons

target L3 pyramidal cells with robust, depressing, perisomatic inhibition.

CCK+ output and MD-evoked FFI are strongly modulated by cannabinoids

A key difference between CCK+ interneurons and PV+ interneurons is that the former often express CB1R on their axon terminals (Katona et al., 1999; Marsicano and Lutz, 1999; Tsou et al., 1999), enabling cannabinoid modulation of CCK+-evoked inhibition. However, CB1R expression levels vary with brain region, the subtype of CCK+ interneuron, and the specific postsynaptic target (Lee et al., 2010; Varga et al., 2010; Vogel et al., 2016). To determine if CCK+ interneurons in PL express CB1R, we examined mRNA expression using fluorescence in situ hybridization (RNAscope) and found that a substantial proportion of EGFP+ cells exhibited strong overlap with CB1R+ mRNA (EGFP+/CB1R+ = 0.62 ± 0.05, $n = 14$ slices, five animals; Fig. 7*A*).

We previously found that cannabinoids selectively modulated CCK+ outputs onto a subset of intratelencephalic (IT) pyramidal cells in L5 of IL (Liu et al., 2020). One possibility is that CCK+ connections onto L3 pyramidal cells in PL, which represent another population of IT cells, could also be cannabinoid sensitive. We evoked CCK+-mediated IPSCs at L3 pyramidal cells every 15 s, held at −50 mV with a low chloride [Cl-] internal solution, which increases the driving force for $GABA_A$ receptor currents and simultaneously captures both EPSCs and IPSCs. We bath applied the CB1R agonist WIN 55,212-1 (WIN, 1 μM) by itself, or in the presence of the CB1R inverse agonist AM-251 (10 μM). We found that WIN significantly reduced CCK+-evoked IPSCs at L3 pyramidal cells compared with baseline after 10 min [Fig. 7*B–D*; baseline ratio WIN = 0.45 (0.28–0.72); WIN vs baseline, $p = 0.0078$; $n = 8$ cells, four animals]. However, in the presence of AM-251, WIN had no effect on CCK+-evoked IPSCs at L3 pyramidal cells [Fig. 7*B–D*; baseline ratio WIN + AM-251 = 1.00 (0.85–1.18); WIN + AM-251 vs baseline AM-251 IPSC, $p = 0.81$; $n = 7$ cells, four animals]. In separate recordings, we also sequentially applied WIN followed by AM-251 and again found that WIN significantly reduced CCK+-evoked IPSCs at L3 pyramidal cells, whereas the application of AM-251 effectively reversed these changes (Extended Data Fig. 7-1*A,B*). These results demonstrate that CCK+ output onto L3 pyramidal cells in PL undergoes robust CB1R-dependent suppression of synaptic transmission that leads to reduced inhibition.

Lastly, having established that CCK+-evoked inhibition is sensitive to CB1R modulation, we examined if this is also the case for MD-evoked FFI. As described above, we expressed ChR2 in MD terminals and recorded L3 pyramidal cells at −50 mV to record compound EPSCs and IPSCs. We found WIN application significantly reduced MD-evoked IPSCs, but not MD-evoked EPSCs [Fig. 7*E,F*: baseline ratio WIN IPSC = 0.48 (0.24–0.98); WIN vs baseline IPSC, $p = 0.031$; WIN EPSC = 0.92 (0.76–1.11); WIN vs baseline EPSC, $p = 0.58$; $n = 7$ cells, four animals]. However, in separate recordings in the presence of AM-251, we found WIN had no effect on either IPSCs or EPSCs [Fig. 7*G,H*; baseline ratio WIN + AM-251 IPSC = 0.93 (0.67–1.29); WIN + AM-251 vs baseline AM-251 IPSC, $p = 0.16$; WIN + AM-251 EPSC = 0.91 (0.78–1.06); WIN + AM-251 vs AM-251 EPSC, $p = 0.43$; $n = 9$ cells, four animals). In another set of recordings, we also performed sequential application of WIN followed by AM-251 and again observed that WIN significantly reduced MD-evoked IPSCs at L3 pyramidal cells, whereas application of AM-251 reversed these changes (Extended Data Fig. 7-1*C,D*). Given the comparable magnitude of IPSC suppression by WIN in both CCK+-evoked IPSCs and MD-evoked FFI, these results suggest that CCK+ interneurons are a major contributor to MD-evoked FFI at pyramidal cells in PL L3.

Discussion

We determined that CCK+ interneurons are major contributors to MD-evoked feed-forward inhibition in PL L3. While PV+ interneurons are relatively sparse in L3 of PL, SOM+, VIP+, and CCK+ interneurons are abundant. There are two electrophysiologically distinct CCK+ populations, with the fast-spiking, basket-like population more strongly activated by MD inputs before other interneuron types. CCK+ interneurons inhibit L3 pyramidal cells perisomatically, exhibit depressing short-term dynamics and are cannabinoid sensitive. Similarly, MD-evoked feed-forward inhibition, but not direct excitation, is also sensitive to CB1R modulation. Our findings shed light on the inhibitory network in PL L3 and highlight how a distinct subset of CCK+ interneurons contribute to MD-evoked FFI. They also suggest how PL is unique compared with other thalamocortical circuits in both sensory systems and the more dorsal, neighboring ACC, with feed-forward inhibition exhibiting prominent sensitivity to cannabinoid signaling.

Throughout the cortex, PV+ interneurons are a major interneuron population and the primary mediator of thalamus-evoked inhibition. While this circuit is present in ACC (Delevich et al., 2015), we found significantly fewer PV+ interneurons in PL L3. Our anatomy is consistent with and extends upon recent analyses of PV+ interneurons across the cortex (Whissell et al., 2015; Kim et al., 2017). Within the PFC, we found, using a variety of approaches, there was a sharp drop-off in L3 PV+ interneurons from ACC to the PL, highlighting distinct cellular makeup. We observed a similar abundance of VIP+ and SOM+ interneurons in L3, unlike previous studies that found fewer VIP+ interneurons than SOM+ interneurons when pooling across layers (Kim et al., 2017), which is likely due to the fact that VIP+ interneurons appear to be enriched in superficial L1-L3 across the cortex (Tremblay et al., 2016). We also found that CCK+ interneurons are enriched in L3 relative to PV+ interneurons, consistent with other studies using different approaches (Kawaguchi and Kubota, 1998; Nguyen et al., 2020). Our results on the distributions of interneuron populations in PL build on previous broad-scale studies on PFC interneurons to highlight laminar specificity.

The two subpopulations of CCK+ interneurons that we found in PL L3 are consistent with CCK+ interneuron diversity in other brain regions. Recent studies have highlighted multiple transcriptionally defined subgroups of CCK+ interneurons in other parts of the cortex (Tasic et al., 2018; Gouwens et al., 2020; (BICCN), 2021; Scala et al., 2021). Similarly, in the hippocampus, CCK+ interneurons encompass multiple subtypes with distinct electrophysiology, morphology, and synaptic connectivity (Daw et al., 2009; Lee et al., 2010). Two of these CCK+ populations, which coexpress either VIP or VGLUT3, are also found in the cortex and the amygdala (Somogyi et al., 2004; Bodor et al., 2005; Omiya et al., 2015; Pelkey et al., 2020). The nfs-CCK + population that we recorded, which displays high input resistance and low maximum firing rate, may be the CCK+/VIP+ subtype that we observed with fluorescence in situ hybridization. In contrast, the fs-CCK+ population that we recorded may be the fast-spiking, basket-like CCK+/VGLUT3+ subtype, corresponding to CCK+/CB1R+ fluorescent population. Notably, we find

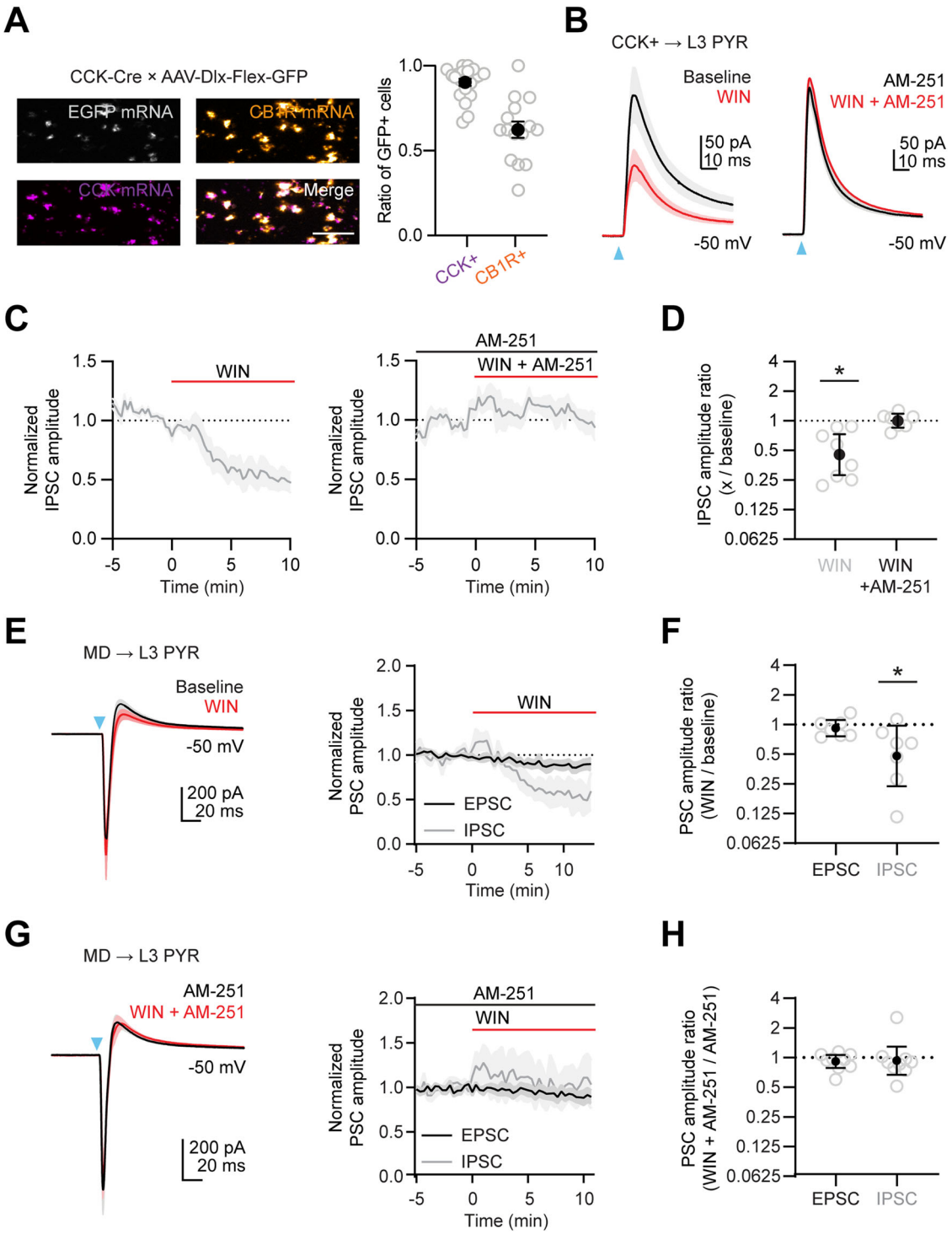

Figure 7. Cannabinoid modulation of CCK ± and MD-evoked FFI. ***A***, Left, Confocal images of EGFP+, CB1R+, and CCK+ mRNA staining in L3 PL of CCK-Cre mice injected with AAV-Dlx-Flex-EGFP. Scale bar = 100 µm. Right, Summary of overlap between EGFP+ (gray) and CCK+ (magenta) or CB1R+ (orange) mRNA ($n = 14$ slices, five animals). ***B***, Left, Average CCK+-evoked IPSCs in L3 PYRs measured at −50 mV at baseline (black) and after wash-in of WIN (red). Blue arrow = 2 ms light pulse. Right, Average CCK+-evoked IPSCs measured at −50 mV, at baseline with AM-251 (black) and after wash-in of WIN (red) in the presence of AM-251. Blue arrow = 2 ms light pulse. ***C***, Time course of CCK+-evoked IPSCs during drug wash-ins, as indicated by colored bars, where IPSCs are normalized to baseline ($n = 8$ cells, four animals). ***D***, Summary of IPSC amplitude ratios during wash-in of WIN (left) or WIN + AM-251 (right). ***E***, Left, Average MD-evoked EPSCs and IPSCs at baseline (black) and after wash-in of WIN (red). Right, Time course of MD-evoked EPSCs (black) and IPSCs (gray) during WIN wash-in, as indicated by the colored bar, where PSCs are normalized to baseline ($n = 7$ cells, four animals). Blue arrow = 2 ms light pulse. ***F***, Summary of EPSC and IPSC amplitude ratio after wash-in of WIN. ***G***, ***H***, Similar to ***E*** and ***F*** in the presence of AM-251 during both baseline and WIN ($n = 9$ cells, four animals). Values are geometric mean and 95% CI. * = $p < 0.05$ (Extended Data Fig. 7-1).

that PL L3 CCK+ interneuron output is fully GABAergic and lacks a glutamatergic component, indicating our approach exclusively targets inhibitory interneurons. While PV+ and CCK+ basket cells are classically considered separate cell types (Freund and Katona, 2007; Tremblay et al., 2016), recent studies have shown an overlap between these two populations (Nguyen

et al., 2020). The intersectional viral strategy we used to label CCK+ cells does not label PV+/CCK+ coexpressing interneurons in CCK-Cre mice. Interestingly, the same strategy may label some of these interneurons in PV-2A-Cre mice, which could be exploited to study this population further. Further exploration of CCK+ subtypes will be essential in disentangling their roles in feed-forward circuits in other regions of the PFC and other cortical areas and determining whether the role of CCK+ interneurons in the PFC is unique or generalizes across other higher cortical regions.

Several of our experiments indicate that CCK+ interneurons make a major contribution to MD-evoked FFI in L3 of PL. MD inputs preferentially activate fs-CCK+ cells over neighboring pyramidal cells but are unable to activate nfs-CCK+ cells. The engagement of fs-CCK+ cells resembles the activation of PV+ basket cells in L3 of ACC and L4 of sensory cortices (Cruikshank et al., 2007; Delevich et al., 2015). It is also similar to hippocampal activation of CCK+ interneurons onto IT cells in L5 of IL (Liu et al., 2020). In contrast, the lack of activation of nsf-CCK+ cells suggests that they are unlikely to contribute to MD-evoked FFI. We recently found MD inputs also engage VIP+ interneurons in L1b of PL, triggering a disinhibitory circuit (Anastasiades et al., 2021). In contrast, MD inputs only weakly targeted VIP+ interneurons in L3, suggesting MD projections to L1b and L3 exhibit markedly different connectivity and function. Previous work from our lab and others also indicates that a variety of long-range inputs can also engage SOM+ interneurons via facilitating synapses (Beierlein et al., 2003; Tan et al., 2008; McGarry and Carter, 2016). While MD inputs also contact SOM+ interneurons in L3, this occurred in tandem with activation of pyramidal cells, making it hard to distinguish from feedback inhibition via activation of the local circuit (Reyes et al., 1998). Taken together, our results suggest that MD inputs strongly engage CCK+ interneurons in L3, highlighting a key role for these cells in prefrontal inhibition.

The study of CCK+ interneurons in the cortex has been hampered by CCK expression in pyramidal cells, which we overcame with intersectional viral tools (Dimidschstein et al., 2016; Nguyen et al., 2020). Our results indicate that CCK+ interneurons synapse strongly near the soma region of L3 pyramidal cells and provide depressing inhibition. These results are again consistent with fs-CCK+ interneurons fulfilling a similar niche to PV+ interneurons in other cortical areas (Karube et al., 2004; Cruikshank et al., 2007). We also determined that CCK+-evoked inhibition is cannabinoid sensitive, which we have previously examined for similar connections in IL L5 (Liu et al., 2020). However, in contrast to CCK+-evoked and hippocampal-evoked inhibition in IL L5, we did not observe robust DSI (Extended Data Fig. 7-1*E*,*F*), consistent with the lack of DSI in other L3 pyramidal cells in the absence of additional pharmacological modulation (Yoshino et al., 2011). One possibility is that L3 pyramidal cells may not produce endocannabinoids as readily as L5 IT cells (Best and Regehr, 2010; Yoshino et al., 2011). In the future, it will be interesting to identify the source of endocannabinoids, including identifying the locations of their synthesis enzymes (Best and Regehr, 2010; Tanimura et al., 2010) and how their expression can be influenced by behavioral experience (Vogel et al., 2016).

The finding that MD-evoked FFI is also suppressed by CB1Rs suggests that CCK+ interneurons contribute to FFI in PL. Other studies have used cell-type specific optogenetic or pharmacogenetic inhibition to link the suppression of a specific interneuron population with the reduction in inhibition (Xu et al., 2013; Delevich et al., 2015; Anastasiades et al., 2021). We used CB1R modulation of CCK+ interneuron output to perform an equivalent loss-of-function experiment (Liu et al., 2020), finding a similar magnitude of reduction for both MD-evoked and CCK+-evoked inhibition at L3 pyramidal cells. This experiment was possible because CB1R is predominantly expressed in CCK+ interneurons in the cortex, and CB1Rs are not found on MD terminals (Herkenham et al., 1990; Matsuda et al., 1993; Marsicano and Lutz, 1999). Consequently, we did not observe CB1R-mediated modulation of MD-evoked excitation at L3 pyramidal cells. While our results cannot rule out the presence of a separate population of CB1R-expressing interneurons, both transcriptomic and immunohistochemical studies of the PFC suggest that there is unlikely to be another major population of CB1R-expressing interneurons (Marsicano and Lutz, 1999; Paul et al., 2017). Together, the activation of CCK+ interneurons, their inhibition of pyramidal cells, and their modulation by CB1Rs support the idea that these cells contribute to MD-evoked FFI in L3 of PL.

Our results suggest CCK+ interneurons in L3 of PL assume some of the functional roles of PV+ interneurons in L4 of the sensory cortex (Gabernet et al., 2005; Cruikshank et al., 2007; Delevich et al., 2015). However, the potent CB1R modulation of both CCK+ and MD-evoked inhibition suggests this circuit may be uniquely modulated. Moreover, the sparsity of PV+ interneurons in L3 of PL suggests they may play a different functional role than is often assumed. Our findings appear to contrast with several in vivo studies showing a prominent role for PV+ interneurons in the PFC (Courtin et al., 2014; Cummings and Clem, 2020; Mukherjee et al., 2021; Cho et al., 2023). It may be that in vivo recordings were made from the small subset of PV+ cells in L3 of PL, from the larger pool of PV+ cells in L5 of PL, or from PV+ cells located in either L3 or L5 of more dorsal areas like ACC (Delevich et al., 2015). Given that fs-CCK+ cells have indistinguishable physiological properties from PV+ cells, it may be challenging to identify them based on firing alone. While our data suggests there are at least two populations of CCK+ interneurons with distinct firing and response properties, in the future, it will be interesting to parse additional subpopulations (Tasic et al., 2018; Gouwens et al., 2020; (BICCN), 2021; Scala et al., 2021).

Lastly, our results suggest that CB1R modulation may play an important role in shaping PFC-dependent behaviors via CCK+ interneurons. Reciprocal loops between the MD and PFC mediate working memory (Bolkan et al., 2017; Schmitt et al., 2017; Mukherjee et al., 2021), and we predict that changes in cannabinoid signaling, mediated in part by CCK+ interneurons, could contribute to disruptions in a variety of cognitive tasks mediated by the PFC. In support of this idea, Δ9-tetrahydrocannabinol (THC), a CB1R agonist, can cause impairments in working memory (Adam et al., 2020). Conversely, reduced endocannabinoid activity could dampen activity in PFC thalamocortical loops via increased output from CCK+ interneurons. These shifts in CCK+ inhibition could be clinically relevant, given that chronic pain leads to excessive synaptic inhibition in the PFC (Woodhams et al., 2017) and reduced endocannabinoid signaling (Mecca et al., 2021), whereas acute stress elevates cannabinoid signaling in the PFC (Hill et al., 2011). In future studies, it will be important to assess the contributions of CCK+ interneurons, their engagement by MD, and their modulation by cannabinoids, in both behaviors and neuropsychiatric disorders associated with the PFC.

References

Adam KCS, Doss MK, Pabon E, Vogel EK, de Wit H (2020) Delta(9)-tetrahydrocannabinol (THC) impairs visual working memory performance: a randomized crossover trial. Neuropsychopharmacology 45:1807–1816.

Anastasiades PG, Carter AG (2021) Circuit organization of the rodent medial prefrontal cortex. Trends Neurosci 44:550–563.

Anastasiades PG, Collins DP, Carter AG (2021) Mediodorsal and ventromedial thalamus engage distinct L1 circuits in the prefrontal cortex. Neuron 109:314–330.e314.

Anastasiades PG, Marlin JJ, Carter AG (2018) Cell-type specificity of callosally evoked excitation and feedforward inhibition in the prefrontal cortex. Cell Rep 22:679–692.

Armstrong C, Soltesz I (2012) Basket cell dichotomy in microcircuit function. J Physiol 590:683–694.

Atallah BV, Bruns W, Carandini M, Scanziani M (2012) Parvalbumin-expressing interneurons linearly transform cortical responses to visual stimuli. Neuron 73:159–170.

Baimel C, Jang E, Scudder SL, Manoocheri K, Carter AG (2022) Hippocampal-evoked inhibition of cholinergic interneurons in the nucleus accumbens. Cell Rep 40:111042.

Beierlein M, Gibson JR, Connors BW (2003) Two dynamically distinct inhibitory networks in layer 4 of the neocortex. J Neurophysiol 90:2987–3000.

Best AR, Regehr WG (2010) Identification of the synthetic pathway producing the endocannabinoid that mediates the bulk of retrograde signaling in the brain. Neuron 65:291–292.

(BICCN), B.I.C.C.N. (2021) A multimodal cell census and atlas of the mammalian primary motor cortex. Nature 598:86–102.

Bodor AL, Katona I, Nyiri G, Mackie K, Ledent C, Hajos N, Freund TF (2005) Endocannabinoid signaling in rat somatosensory cortex: laminar differences and involvement of specific interneuron types. J Neurosci 25: 6845–6856.

Bolkan SS, Stujenske JM, Parnaudeau S, Spellman TJ, Rauffenbart C, Abbas AI, Harris AZ, Gordon JA, Kellendonk C (2017) Thalamic projections sustain prefrontal activity during working memory maintenance. Nat Neurosci 20:987–996.

Chalifoux JR, Carter AG (2010) GABAB receptors modulate NMDA receptor calcium signals in dendritic spines. Neuron 66:101–113.

Cho KKA, Shi J, Phensy AJ, Turner ML, Sohal VS (2023) Long-range inhibition synchronizes and updates prefrontal task activity. Nature 617:548–554.

Collins DP, Anastasiades PG, Marlin JJ, Carter AG (2018) Reciprocal circuits linking the prefrontal cortex with dorsal and ventral thalamic nuclei. Neuron 98:366–379 e364.

Courtin J, Chaudun F, Rozeske RR, Karalis N, Gonzalez-Campo C, Wurtz H, Abdi A, Baufreton J, Bienvenu TC, Herry C (2014) Prefrontal parvalbumin interneurons shape neuronal activity to drive fear expression. Nature 505:92–96.

Cruikshank SJ, Lewis TJ, Connors BW (2007) Synaptic basis for intense thalamocortical activation of feedforward inhibitory cells in neocortex. Nat Neurosci 10:462–468.

Cruikshank SJ, Urabe H, Nurmikko AV, Connors BW (2010) Pathway-specific feedforward circuits between thalamus and neocortex revealed by selective optical stimulation of axons. Neuron 65:230–245.

Cummings KA, Clem RL (2020) Prefrontal somatostatin interneurons encode fear memory. Nat Neurosci 23:61–74.

Daw MI, Tricoire L, Erdelyi F, Szabo G, McBain CJ (2009) Asynchronous transmitter release from cholecystokinin-containing inhibitory interneurons is widespread and target-cell independent. J Neurosci 29:11112–11122.

Delevich K, Tucciarone J, Huang ZJ, Li B (2015) The mediodorsal thalamus drives feedforward inhibition in the anterior cingulate cortex via parvalbumin interneurons. J Neurosci 35:5743–5753.

Dienel SJ, Lewis DA (2019) Alterations in cortical interneurons and cognitive function in schizophrenia. Neurobiol Dis 131:104208.

Dimidschstein J, et al. (2016) A viral strategy for targeting and manipulating interneurons across vertebrate species. Nat Neurosci 19:1743–1749.

Euston DR, Gruber AJ, McNaughton BL (2012) The role of medial prefrontal cortex in memory and decision making. Neuron 76:1057–1070.

Freund TF, Katona I (2007) Perisomatic inhibition. Neuron 56:33–42.

Gabernet L, Jadhav SP, Feldman DE, Carandini M, Scanziani M (2005) Somatosensory integration controlled by dynamic thalamocortical feedforward inhibition. Neuron 48:315–327.

Gentet LJ, Kremer Y, Taniguchi H, Huang ZJ, Staiger JF, Petersen CC (2012) Unique functional properties of somatostatin-expressing GABAergic neurons in mouse barrel cortex. Nat Neurosci 15:607–612.

Glickfeld LL, Scanziani M (2006) Distinct timing in the activity of cannabinoid-sensitive and cannabinoid-insensitive basket cells. Nat Neurosci 9:807–815.

Gouwens NW, et al. (2020) Integrated morphoelectric and transcriptomic classification of cortical GABAergic cells. Cell 183:935–953.e919.

Halassa MM, Sherman SM (2019) Thalamocortical circuit motifs: a general framework. Neuron 103:762–770.

He M, et al. (2016) Strategies and tools for combinatorial targeting of GABAergic neurons in mouse cerebral cortex. Neuron 91:1228–1243.

Herkenham M, Lynn AB, Little MD, Johnson MR, Melvin LS, de Costa BR, Rice KC (1990) Cannabinoid receptor localization in brain. Proc Natl Acad Sci U S A 87:1932–1936.

Hill MN, et al. (2011) Recruitment of prefrontal cortical endocannabinoid signaling by glucocorticoids contributes to termination of the stress response. J Neurosci 31:10506–10515.

Hippenmeyer S, Vrieseling E, Sigrist M, Portmann T, Laengle C, Ladle DR, Arber S (2005) A developmental switch in the response of DRG neurons to ETS transcription factor signaling. PLoS Biol 3:e159.

Karnani MM, Jackson J, Ayzenshtat I, Hamzehei Sichani A, Manoocheri K, Kim S, Yuste R (2016) Opening holes in the blanket of inhibition: localized lateral disinhibition by VIP interneurons. J Neurosci 36:3471–3480.

Karube F, Kubota Y, Kawaguchi Y (2004) Axon branching and synaptic bouton phenotypes in GABAergic nonpyramidal cell subtypes. J Neurosci 24: 2853–2865.

Katona I, Sperlagh B, Sik A, Kafalvi A, Vizi ES, Mackie K, Freund TF (1999) Presynaptically located CB1 cannabinoid receptors regulate GABA release from axon terminals of specific hippocampal interneurons. J Neurosci 19:4544–4558.

Kawaguchi Y, Kubota Y (1998) Neurochemical features and synaptic connections of large physiologically-identified GABAergic cells in the rat frontal cortex. Neuroscience 85:677–701.

Kim Y, et al. (2017) Brain-wide maps reveal stereotyped cell-type-based cortical architecture and subcortical sexual dimorphism. Cell 171:456–469 e422.

Krettek JE, Price JL (1977) The cortical projections of the mediodorsal nucleus and adjacent thalamic nuclei in the rat. J Comp Neurol 171: 157–191.

Kuramoto E, Pan S, Furuta T, Tanaka YR, Iwai H, Yamanaka A, Ohno S, Kaneko T, Goto T, Hioki H (2017) Individual mediodorsal thalamic neurons project to multiple areas of the rat prefrontal cortex: a single neuron-tracing study using virus vectors. J Comp Neurol 525:166–185.

Lee SH, Foldy C, Soltesz I (2010) Distinct endocannabinoid control of GABA release at perisomatic and dendritic synapses in the hippocampus. J Neurosci 30:7993–8000.

Lee S, Kruglikov I, Huang ZJ, Fishell G, Rudy B (2013) A disinhibitory circuit mediates motor integration in the somatosensory cortex. Nat Neurosci 16: 1662–1670.

Lewis DA, Curley AA, Glausier JR, Volk DW (2012) Cortical parvalbumin interneurons and cognitive dysfunction in schizophrenia. Trends Neurosci 35:57–67.

Liu X, Dimidschstein J, Fishell G, Carter AG (2020) Hippocampal inputs engage CCK+ interneurons to mediate endocannabinoid-modulated feed-forward inhibition in the prefrontal cortex. Elife 9:e55267.

Madisen L, et al. (2010) A robust and high-throughput Cre reporting and characterization system for the whole mouse brain. Nat Neurosci 13: 133–140.

Manoocheri K, Carter AG (2022) Rostral and caudal basolateral amygdala engage distinct circuits in the prelimbic and infralimbic prefrontal cortex. Elife 11:e82688.

Marlin JJ, Carter AG (2014) GABA-A receptor inhibition of local calcium signaling in spines and dendrites. J Neurosci 34:15898–15911.

Marsicano G, Lutz B (1999) Expression of the cannabinoid receptor CB1 in distinct neuronal subpopulations in the adult mouse forebrain. Eur J Neurosci 11:4213–4225.

Matsuda LA, Bonner TI, Lolait SJ (1993) Localization of cannabinoid receptor mRNA in rat brain. J Comp Neurol 327:535–550.

McGarry LM, Carter AG (2016) Inhibitory gating of basolateral amygdala inputs to the prefrontal Cortex. J Neurosci 36:9391–9406.

McGarry LM, Packer AM, Fino E, Nikolenko V, Sippy T, Yuste R (2010) Quantitative classification of somatostatin-positive neocortical interneurons identifies three interneuron subtypes. Front Neural Circuits 4:12.

Mecca CM, et al. (2021) Dynamic change of endocannabinoid signaling in the medial prefrontal cortex controls the development of depression after neuropathic pain. J Neurosci 41:7492–7508.

Mukherjee A, Lam NH, Wimmer RD, Halassa MM (2021) Thalamic circuits for independent control of prefrontal signal and noise. Nature 600:100–104.

Nguyen R, Venkatesan S, Binko M, Bang JY, Cajanding JD, Briggs C, Sargin D, Imayoshi I, Lambe EK, Kim JC (2020) Cholecystokinin-expressing interneurons of the medial prefrontal cortex mediate working memory retrieval. J Neurosci 40:2314–2331.

Omiya Y, Uchigashima M, Konno K, Yamasaki M, Miyazaki T, Yoshida T, Kusumi I, Watanabe M (2015) VGluT3-expressing CCK-positive basket cells construct invaginating synapses enriched with endocannabinoid signaling proteins in particular cortical and cortex-like amygdaloid regions of mouse brains. J Neurosci 35:4215–4228.

Parnaudeau S, Bolkan SS, Kellendonk C (2018) The mediodorsal thalamus: an essential partner of the prefrontal Cortex for cognition. Biol Psychiatry 83:648–656.

Paul A, Crow M, Raudales R, He M, Gillis J, Huang ZJ (2017) Transcriptional architecture of synaptic communication delineates GABAergic neuron identity. Cell 171:522–539.e520.

Pelkey KA, et al. (2020) Paradoxical network excitation by glutamate release from VGluT3(+) GABAergic interneurons. Elife 9:e51996.

Petreanu L, Mao T, Sternson SM, Svoboda K (2009) The subcellular organization of neocortical excitatory connections. Nature 457:1142–1145.

Porter JT, Johnson CK, Agmon A (2001) Diverse types of interneurons generate thalamus-evoked feedforward inhibition in the mouse barrel cortex. J Neurosci 21:2699–2710.

Reyes A, Lujan R, Rozov A, Burnashev N, Somogyi P, Sakmann B (1998) Target-cell-specific facilitation and depression in neocortical circuits. Nat Neurosci 1:279–285.

Rudy B, Fishell G, Lee S, Hjerling-Leffler J (2011) Three groups of interneurons account for nearly 100% of neocortical GABAergic neurons. Dev Neurobiol 71:45–61.

Scala F, et al. (2021) Phenotypic variation of transcriptomic cell types in mouse motor cortex. Nature 598:144–150.

Schmitt LI, Wimmer RD, Nakajima M, Happ M, Mofakham S, Halassa MM (2017) Thalamic amplification of cortical connectivity sustains attentional control. Nature 545:219–223.

Scudder SL, Baimel C, Macdonald EE, Carter AG (2018) Hippocampal-evoked feedforward inhibition in the nucleus accumbens. J Neurosci 38:9091–9104.

Silberberg G, Markram H (2007) Disynaptic inhibition between neocortical pyramidal cells mediated by Martinotti cells. Neuron 53:735–746.

Somogyi J, Baude A, Omori Y, Shimizu H, El Mestikawy S, Fukaya M, Shigemoto R, Watanabe M, Somogyi P (2004) GABAergic basket cells expressing cholecystokinin contain vesicular glutamate transporter type 3 (VGLUT3) in their synaptic terminals in hippocampus and isocortex of the rat. Eur J Neurosci 19:552–569.

Tan Z, Hu H, Huang ZJ, Agmon A (2008) Robust but delayed thalamocortical activation of dendritic-targeting inhibitory interneurons. Proc Natl Acad Sci U S A 105:2187–2192.

Taniguchi H, et al. (2011) A resource of Cre driver lines for genetic targeting of GABAergic neurons in cerebral cortex. Neuron 71:995–1013.

Tanimura A, et al. (2010) The endocannabinoid 2-arachidonoylglycerol produced by diacylglycerol lipase alpha mediates retrograde suppression of synaptic transmission. Neuron 65:320–327.

Tasic B, et al. (2018) Shared and distinct transcriptomic cell types across neocortical areas. Nature 563:72–78.

Tremblay R, Lee S, Rudy B (2016) GABAergic interneurons in the neocortex: from cellular properties to circuits. Neuron 91:260–292.

Tsou K, Mackie K, Sañudo-Peña MC, Walker JM (1999) Cannabinoid CB1 receptors are localized primarily on cholecystokinin-containing GABAergic interneurons in the rat hippocampal formation. Neuroscience 93:969–975.

Varga C, Lee SY, Soltesz I (2010) Target-selective GABAergic control of entorhinal cortex output. Nat Neurosci 13:822–824.

Vogel E, Krabbe S, Grundemann J, Wamsteeker Cusulin JI, Luthi A (2016) Projection-specific dynamic regulation of inhibition in amygdala microcircuits. Neuron 91:644–651.

Wang F, Flanagan J, Su N, Wang LC, Bui S, Nielson A, Wu X, Vo HT, Ma XJ, Luo Y (2012) RNAscope: a novel in situ RNA analysis platform for formalin-fixed, paraffin-embedded tissues. J Mol Diagn 14:22–29.

Whissell PD, Cajanding JD, Fogel N, Kim JC (2015) Comparative density of CCK- and PV-GABA cells within the cortex and hippocampus. Front Neuroanat 9:124.

Wilson RI, Kunos G, Nicoll RA (2001) Presynaptic specificity of endocannabinoid signaling in the hippocampus. Neuron 31:453–462.

Wilson RI, Nicoll RA (2001) Endogenous cannabinoids mediate retrograde signalling at hippocampal synapses. Nature 410:588–592.

Woodhams SG, Chapman V, Finn DP, Hohmann AG, Neugebauer V (2017) The cannabinoid system and pain. Neuropharmacology 124:105–120.

Xu H, Jeong HY, Tremblay R, Rudy B (2013) Neocortical somatostatin-expressing GABAergic interneurons disinhibit the thalamorecipient layer 4. Neuron 77:155–167.

Yoshino H, et al. (2011) Postsynaptic diacylglycerol lipase mediates retrograde endocannabinoid suppression of inhibition in mouse prefrontal cortex. J Physiol 589:4857–4884.

Zucker RS, Regehr WG (2002) Short-term synaptic plasticity. Annu Rev Physiol 64:355–405.